# Phonon-interface scattering in multilayer graphene on an amorphous support

Mir Mohammad Sadeghi[a], Insun Jo[a], and Li Shi[a,b,1]

[a]Department of Mechanical Engineering and [b]Texas Materials Institute, The University of Texas at Austin, Austin, TX 78712

The recent studies of thermal transport in suspended, supported, and encased graphene just began to uncover the richness of two-dimensional phonon physics, which is relevant to the performance and reliability of graphene-based functional materials and devices. Among the outstanding questions are the exact causes of the suppressed basal-plane thermal conductivity measured in graphene in contact with an amorphous material, and the layer thickness needed for supported or embedded multilayer graphene (MLG) to recover the high thermal conductivity of graphite. Here we use sensitive in-plane thermal transport measurements of graphene samples on amorphous silicon dioxide to show that full recovery to the thermal conductivity of the natural graphite source has yet to occur even after the MLG thickness is increased to 34 layers, considerably thicker than previously thought. This seemingly surprising finding is explained by long intrinsic scattering mean free paths of phonons in graphite along both basal-plane and cross-plane directions, as well as partially diffuse scattering of MLG phonons by the MLG-amorphous support interface, which is treated by an interface scattering model developed for highly anisotropic materials. Based on the phonon transmission coefficient calculated from reported experimental thermal interface conductance results, phonons emerging from the interface consist of a large component that is scattered across the interface, making rational choice of the support materials a potential approach to increasing the thermal conductivity of supported MLG.

phonon transport | boundary scattering | nanoscale thermal transport | two-dimensional materials | thermal management

As a monoatomic layer of carbon atoms arranged in a hexagonal lattice, single-layer graphene (SLG) is the building block of graphite and carbon nanotubes (CNTs), which can be envisioned as a stack of a large number of graphene layers and rolled-up cylinders of graphene sheets, respectively. Thermal transport in these graphitic materials has intrigued researchers for several decades. The industrial use of graphite in high-temperature or high-heat flux applications motivated a number of initial studies of its thermal properties. These studies have found highly anisotropic thermal transport properties in graphite, where the basal-plane thermal conductivity is among the highest found in solids and nearly two orders of magnitude larger than the value measured along the c-axis (1–3). The recent rediscoveries of CNTs and SLG have expanded the applications of these graphitic nanomaterials for electronic devices, sensors, and light-weight composite materials, among others (4, 5). The performance and reliability of CNT and graphene devices are often closely related to the thermal properties of these nanoscale building blocks, similar to the situation in silicon nanoelectronic devices where localized heating has become a grand challenge (6). Hence, there have been a number of studies of thermal transport in these carbon nanostructures. Some of the studies have yielded higher thermal conductivity values in suspended CNTs and graphene than the largest reported graphite value (7, 8). Because of the ultrahigh thermal conductivity and the large surface-to-volume ratio, there have been a large number of efforts in the development of thermal management materials using these carbon nanomaterials (9, 10). However, in most of these applications, graphene and CNTs are either supported on a substrate or embedded in a medium, instead of being suspended. Hence, the effect of interface interaction on phonon transport in and across graphene and CNTs must be understood.

Recently, it has been found that the basal-plane thermal conductivity of SLG or bilayer graphene (BLG) in contact with an amorphous inorganic or organic layer is a factor of three to five lower than those found in high-quality graphite and suspended graphene at room temperature (11, 12). The suppression has been attributed to interface scattering or damping of phonons in graphene, especially the flexural modes that may make a large contribution to the basal-plane thermal conductivity in suspended graphene (13). Another measurement of few-layer graphene (FLG) encased in amorphous oxide has yielded decreasing basal-plane thermal conductivity with decreasing FLG layer thickness (14), opposite to the finding for suspended FLG (8, 15). However, the uncertainty in the experimental data makes it difficult to determine accurately the layer thickness needed for the encased FLG to recover the basal-plane thermal conductivity of graphite. Better understanding of this layer thickness dependence is needed for rational design of FLG lateral heat spreaders for high-power density nanoelectronic devices, and high-surface-area FLG fillers to enhance the thermal conductivity of polymeric composites, among other applications. In addition, there remain questions regarding whether the thermal conductivity reduction is mainly caused by transmission or leakage of phonons across the interface (11, 16), phonon scattering by interface roughness (11, 14), or defects created in the FLG in the sample fabrication processes (10, 14).

Molecular dynamics (MD) simulations have provided insights into the effects of interface interactions on phonon transport in graphene. For instance, MD calculation results have verified that

## Significance

The thermal conductivity of suspended graphene can be even higher than the basal-plane value of graphite, which is among the highest found in solids. However, when graphene is in contact with an amorphous material, the thermal conductivity is suppressed considerably. This paper reports that the thickness of multilayer graphene supported on an amorphous substrate needs to be more than 30 atomic layers to recover the graphite thermal conductivity. The finding is explained by long phonon mean free paths in graphite even along the cross-plane direction, and is used to clarify interface leakage of phonons as an important mechanism for the observed suppression. The result is relevant for the application of graphene for electronics, thermal management, and other applications.

APPLIED PHYSICAL SCIENCES

flexural phonons make an important contribution to the thermal conductivity in suspended graphene, and this contribution is considerably suppressed by an amorphous support (17–19). In addition, a recent MD simulation has shown increasing thermal conductivity with increasing layer thickness of FLG supported on amorphous $SiO_2$ (19). The result suggests a rapid increase of the basal-plane thermal conductivity to approach 90% of the graphite value when the FLG thickness increases to about six layers. However, the accuracy in classical MD simulation results has been limited by the lack of effective quantum correction methods and high-fidelity interatomic potentials for graphitic systems (20), where the specific heat is still considerably lower than the classical limit even at room temperature because of high Debye temperature of graphite. In addition, although a MD simulation suggests such role is negligible for a single-wall CNT supported on an amorphous support (21), the role of phonon leakage (11, 16) across the interface in the thermal conductivity of supported graphene remains to be elusive.

To clarify these outstanding questions, here we report results from temperature-dependent thermal conductivity measurements of FLG and multilayer graphene (MLG) supported on $SiO_2$ and the natural graphite (NG) source used to exfoliate the FLG and MLG samples. Compared with the measurement values for encased FLG (14) and MD simulation data for supported FLG (19), the measurement results suggest a rather gradual convergence of the MLG basal-plane thermal conductivity to the graphite value when the MLG layer thickness is increased, especially at low temperatures. A shift of the peak thermal conductivity toward a higher temperature is observed in the thinner supported MLG samples. Accounting for the highly anisotropic phonon dispersion in MLG, solutions of phonon Boltzmann transport equation are developed to analyze the measurement results of the basal-plane thermal conductivity and interface thermal conductance of MLG on amorphous oxide support and the anisotropic thermal conductivities of graphite. Based on the analysis, the observed gradual convergence and peak shift can be well explained by long intrinsic mean free paths of phonons in graphite and partially diffuse phonon-interface scattering in the supported MLG. Moreover, such partially diffuse interface scattering process is influenced by a rather large transmission component, especially for low-frequency phonons that make a large contribution to the peak thermal conductivity of graphite at low temperatures and possess high interface transmission coefficient in supported graphene.

## Results

Five MLG samples have been measured in this work, and are referred hereafter as G2, G6, G8, G27, and G34, where the number represents the layer thickness (see *SI Materials and Methods* for sample dimensions). These MLG samples are supported on 300-nm-thick suspended $SiO_2$ bridges. As shown in Fig. 1, each end of the central $SiO_2$ bridge is connected to one straight Cr/Au line and one U-shape Cr/Au line supported on suspended 300-nm-thick $SiO_2$ beams. The metal lines are used as resistance thermometers (RTs) in the thermal measurement (11) (*Materials and Methods* and *SI Materials and Methods*). In addition, the basal-plane thermal conductivity of the NG source used to exfoliate the MLG samples has also been measured using a steady-state comparative method.

As shown in Fig. 2 and Fig. 3, the thermal conductivity of the FLG and MLG samples supported on $SiO_2$ increases with the layer thickness in the thickness range between 1 and 34 atomic layers, and has not yet reached the basal-plane thermal conductivity of the NG source used to exfoliate the MLG samples. The convergence to the graphite value is considerably more gradual than the prediction of a recent MD simulation (19). The observed thickness dependence is opposite and qualitatively similar to the reported behaviors of suspended FLG (8, 15) and
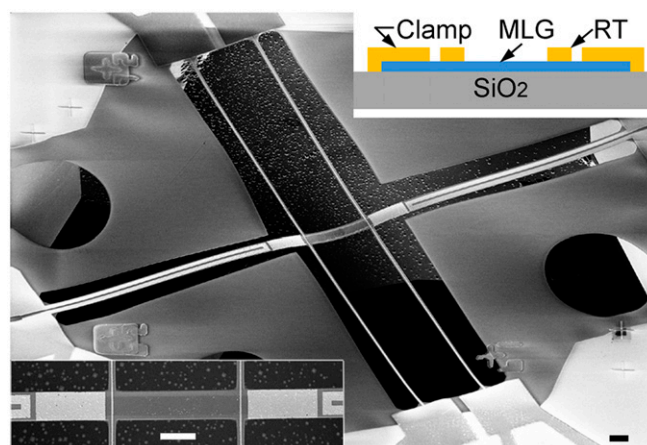


**Fig. 1.** Scanning electron micrograph of the MLG sample G34 at a 45° view angle. The top and bottom insets show schematic cross-section and top view of the central bridge, respectively. (Scale bar, 10 μm.)

FLG encased in $SiO_2$ (14), respectively (Fig. 3). For suspended FLG, results from a micro-Raman measurement (8) and a theoretical calculation (15) both suggest that interlayer phonon scattering decreases the thermal conductivity to approach the basal-plane value of graphite when the suspended FLG layer thickness is increased to only about four layers.

Moreover, the thermal conductivity peak is shifted to a lower temperature for a thicker supported FLG sample. Such peak shifts have not been resolved in the earlier studies of suspended FLG (8) and encased FLG (14). In comparison, the peak thermal conductivity occurs at an even lower temperature of ∼100 K for high-quality pyrolytic graphite (PG) (2) and the NG source used to exfoliate the graphene samples. As the temperature increases to above room temperature, the thermal conductivity of G34 becomes comparable to that of the NG source (Fig. 2).

## Discussions

To identify the causes of the observed thickness and temperature dependences in the thermal conductivity of supported MLG, we have examined a number of possible mechanisms. We first rule out phonon scattering by the lateral edges of the MLG flakes as the main cause for the suppressed thermal conductivity. The smallest lateral dimension of the MLG flakes is as large as 3 μm, which would have yielded much higher thermal conductivity than the measurement results if diffuse edge scattering was the dominant mechanism, as shown in ref. 12 and the calculation discussed below. Similarly, scattering by point defects inside the graphene lattice cannot explain the thickness dependence, because the D band associated with point defects (22) cannot be observed in the Raman spectra of all of the MLG samples, which were exfoliated from the same graphite source and underwent the same sample preparation steps. Hence, the experimental result needs to be attributed to the interaction between the MLG and the underlying $SiO_2$ support, and also possibly polymer residue left on the top surface from the device fabrication process (12, 23). The van der Waals (vdW) interaction between graphene and an amorphous layer can result in perturbation of the atomic bonding in the graphene layers near the interface. Such vdW interaction is known to be short range. For example, the interface adhesion energy between FLG and $SiO_2$ was found to saturate for FLG samples thicker than two layers (24), suggesting that the static force interaction at the interface only affects the layer adjacent to the substrate. The short-range perturbation can modify the group velocities of phonons in the graphene layer next to the interface. For strong interfacial bonding between SLG and Ni (111) (25, 26) or Ru (27), softening of the optical branches and
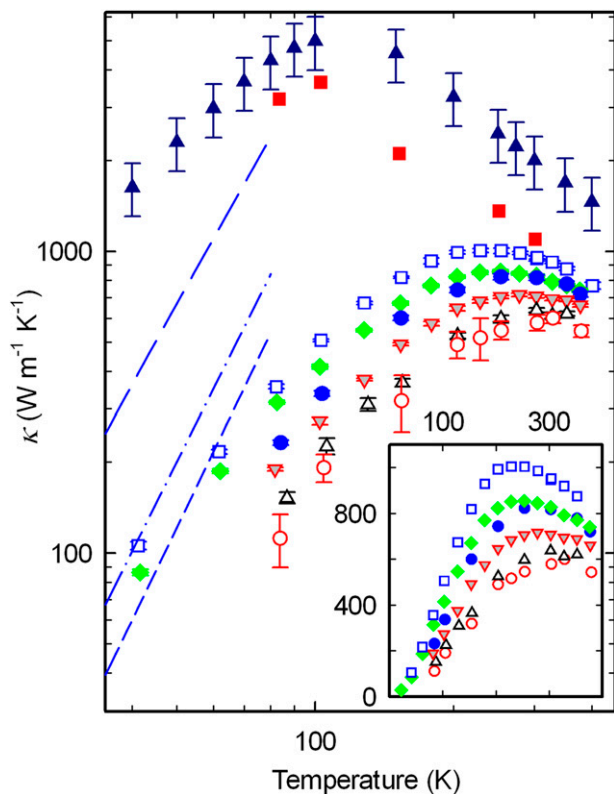
**Fig. 2.** Measured basal-plane thermal conductivity as a function of temperature for single-layer (11) (red unfilled circles), bilayer (black unfilled triangles), six-layer (gray filled inverted red triangles), eight-layer (blue filled circles), 27-layer (green filled diamonds), and 34-layer (blue unfilled squares) graphene supported on SiO2. Also shown for comparison are the thermal conductivity of the NG source of the MLG samples (red filled squares) and the highest reported graphite thermal conductivity values included in Touloukian et al. (2) (dark blue filled triangles). The lines are the calculated low-temperature thermal conductivity of a 34-layer MLG with dimensions similar to the 34-layer MLG sample with diffuse top and bottom surfaces (blue short dashed line), specular top surface and diffuse bottom surface (blue dot dashed line), and partially diffuse top and bottom surfaces with the same specularity parameter of 0.36 (blue dot dashed line) or 0.9 (blue long dashed line). The two side edges are treated as diffuse, and other scattering mechanisms are ignored in the calculation. The inset shows that the measured thermal conductivities of the supported MLG increases with increasing thickness, with the peak value shifted to a lower temperature for a thicker sample.

modification of the flexural phonon branch have been observed. However, as the interface bonding was weakened by intercalation of another layer of Cu or Ag at the interface (26, 28) or for the case of SLG physisorbed on a Pt substrate (29), the phonon dispersion of supported SLG becomes similar to that of pristine graphite. The adhesion energies for SLG–SiO2 and FLG–SiO2 interfaces have been determined to be 0.45 J·m$^{-2}$ and 0.31 J·m$^{-2}$, respectively (24), smaller than the 0.72 J·m$^{-2}$ value reported for SLG–Cu interface (30). Hence, we expect that the weak and short-range vdW interaction is insufficient to cause appreciable reduction of the group velocities of those phonon modes that dominate the thermal conductivity in suspended MLG. Therefore, static perturbation of the atomic bonding and modification of the phonon dispersion in the few graphene layers near the interface alone cannot explain the observed long-range effect, namely the reduced thermal conductivity in the 34-layer MLG sample, especially the pronounced reduction at low temperatures.

Nevertheless, the short-range vdW interaction at the interface can still result in ripples throughout the supported MLG. SLG was found to be rather conformal to the surface roughness of a

SiO2 support (31, 32). The roughness of graphene supported on SiO2 was found to decrease from 185 pm to 125 pm when the thickness increases from single layer to 15 layers (24). Fitting of the thickness-dependent surface roughness data yields a surface roughness of 123 pm for graphite of infinite number of graphene layers. In addition, with increasing thickness from SLG to BLG and three-layer graphene, the substrate-induced surface roughness decreases by 50% and 70%, respectively. Such substrate-induced surface roughness for the supported FLG is comparable in amplitude and wavelength to the intrinsic ripples (33) in suspended SLG and FLG, where both the ripple amplitude (34) and thermal conductivity (8) decrease with increasing layer thickness. Hence, substrate-induced ripples cannot explain the greatly suppressed magnitude and opposite thickness dependence in the measured thermal conductivity of the supported MLG. Similarly, stress and adhesion energy variations in the MLG samples are not expected to play a major role, as discussed in *SI Materials and Methods*.

We next consider the dynamic nature of the interface interaction. The average mean free path of phonons in graphite along a direction $\alpha$, $\Lambda_\alpha$, can be calculated from:

$$\Lambda_\alpha^{-1} = \frac{1}{\kappa_\alpha} \sum_p \sum_{\vec{k}} |v_\alpha| k_B \, x^2 \frac{e^x}{(e^x-1)^2} \frac{\Delta k^3}{8\pi^3}, \quad x \equiv \hbar\omega/k_B T, \qquad [1]$$

where the summations are over all phonon polarizations ($p$) and wave vector ($\vec{k}$) states in a discretized Brillouin zone, $\Delta k^3$ is the volume of each grid within the discretized Brillouin zone, $\hbar$ is the reduced Planck constant, $\omega$ is the angular frequency, $k_B$ is the Boltzmann constant, $T$ is the temperature, and $\kappa_\alpha$ and $v_\alpha$ are the thermal conductivity and phonon group velocity component along direction $\alpha$. We have calculated the full phonon dispersion of graphite based on the density functional perturbation theory with the use of ab initio calculation package QUANTUM ESPRESSO (35), and used a numerical approach to carry out the summation of Eq. **1** in the discretized Brillouin zone of graphite (*SI Materials and Methods*). Based on the reported cross-plane
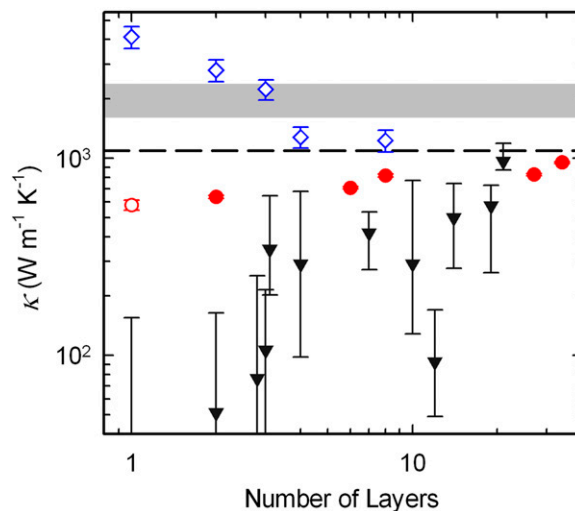


**Fig. 3.** Basal-plane thermal conductivity of SLG (red unfilled circle) (11) and MLG supported on SiO2 (red filled circles) as a function of layer thickness at 300 K. Also shown for comparison are the thermal conductivity of suspended SLG and FLG samples (blue unfilled diamonds) reported by Ghosh et al. (8), FLG samples encased in SiO2 (black filled inverted triangles) reported by Jang et al. (14), the NG source of the MLG samples (dashed line), and the highest reported graphite thermal conductivity values (gray shaded area) included in Touloukian et al. (2).

thermal conductivity of graphite (2), $\Lambda_z$ was found to increase with decreasing temperature, from more than 60 atomic layers at 300 K to over 1,000 atomic layers at temperatures lower than 70 K, as shown in Fig. 4. The as-calculated $\Lambda_z$ value at temperature 300 K, about 20 nm, is comparable to the 10 nm value estimated from the simplified Kinetic theory in a recent work (36). In addition, the average basal-plane mean free path calculated with this approach is even much longer than the cross-plane values, and approaches about 240 nm at room temperature, which is about one-third of the 775 nm value suggested for suspended graphene (10) based on the simplified Kinetic theory and a graphene thermal conductivity value up to a factor of 2.6 higher than the graphite basal-plane value used here. This calculation based on Eq. 1 has not accounted for the frequency dependence of the phonon mean free path. According to Klemens (37), the phonon–phonon scattering mean free path in the basal plane of graphene and graphite depends on $\omega$ and $T$ according to $\Lambda \sim T^{-1}\omega^{-2}$. Because low-frequency acoustic phonons possess longer mean free paths and make larger contributions to the thermal conductivity than optical phonons, the average phonon mean free path weighted by the thermal conductivity contribution is expected to be even larger than the values found from Eq. 1. The large $\Lambda_z$ values suggest that phonons originating from graphene layers far away from the interface can be scattered by the interface before other intrinsic scattering events occur. Such scattering at the top and bottom interfaces result in a reduction of the basal-plane phonon mean free path. If the top and bottom surfaces are diffuse, the basal-plane phonon mean free path due to scattering at the two surfaces is proportional to the MLG layer thickness and the ratio between the $ab$-plane component ($v_a$) and $c$-axis component ($v_z$) of the phonon group velocity (37).

We have conducted theoretical calculation to investigate whether the measurement results can be attributed to partially diffuse phonon scattering at the top and bottom surfaces. Phonon scattering at the MLG–SiO$_2$ interface is complicated by the highly anisotropic phonon dispersion in MLG and phonon transmission across the interface. Because of the anisotropic structure, the phonon group velocity is not collinear with the phase velocity, and has a much larger $v_a$ component than the $v_z$ component for most of the phonon modes. For thick MLG, the average phonon transmission coefficient from MLG to SiO$_2$ can be evaluated from the thermal interface conductance ($G_c$) according to (38, 39):
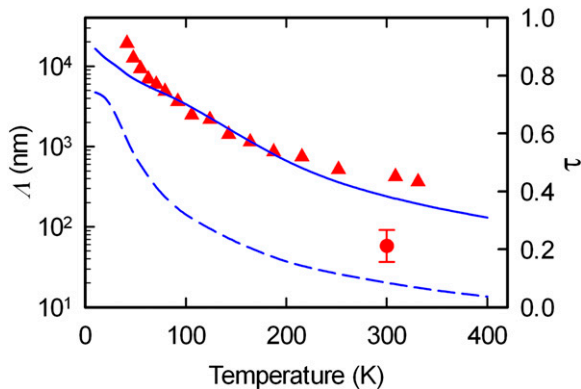


**Fig. 4.** Calculated average phonon mean free path ($\Lambda$) in graphite along the basal-plane (blue solid line) and cross-plane (blue dashed line) directions. The mean free path of phonons that dominates the thermal conductivity is expected to be longer than the shown average mean free path. Also shown is the calculated average interface phonon transmission coefficient ($\tau$) from FLG to SiO$_2$ based on the measured FLG–SiO$_2$ thermal interface conductance values reported by Chen et al. (41) for a 3-nm-thick FLG (red filled triangles) and Mak et al. (40) (red filled circle).

$$\tau_{MLG \to SiO_2} = G_c \left( \sum_p \sum_{\vec{k}, k_z < 0} |v_z| \ k_B \ x^2 \frac{e^x}{(e^x - 1)^2} \frac{\Delta k^3}{8\pi^3} \right)^{-1}. \quad [2]$$

Based on the reported $G_c$ value measured for FLG supported on SiO$_2$ (40), this calculation yields a $\tau_{MLG \to SiO_2}$ value of about 0.2 near room temperature. The use of the measured $G_c$ value reported by Chen et al. (41) for encased FLG yields even higher $\tau_{MLG \to SiO_2}$ values, which increase with decreasing temperature, as shown in Fig. 4. This calculation is not applicable for SLG and thin FLG supported on SiO$_2$, where $v_z$ vanishes because of the absence of cross-plane modes. However, the measured $G_c$ value for SLG–SiO$_2$ interface is comparable to that for MLG–SiO$_2$ (40), suggesting coupling between some in-plane modes in SLG and surface and bulk modes in SiO$_2$.

Because of phonon scattering across the interface, MLG phonons emerging from the interface consist of a reflection component and a transmitted component from the adjacent amorphous layer. Because the temperature gradient is parallel to the interface, the transmitted component from the amorphous layer into the MLG is balanced by phonons scattered from MLG into the amorphous layer, so that the net interface heat flux is zero. In addition, phonons transmitted from or into the amorphous layer are expected to be highly diffuse because of atomic scale mean free path in the amorphous layer.

We have derived an analytical model for thermal conductivity of supported MLG in the boundary scattering regime, which cannot be treated by existing models established for an isotropic thin film (42). In the following, the temperature gradient is along the $x$-axis that is parallel to the basal plane, and the $z$-axis is along the $c$-axis of graphite. In this coordinate, $\theta$ and $\varphi$ are the polar angle with $x$-axis and its corresponding azimuthal angle in the $yz$-plane, respectively (Fig. 5). The deviation of the distribution function $f$ of phonons with wave vector $\vec{k}$ from the local equilibrium $f_0$ at any point $A$ in the MLG is obtained as:

$$g_A\left(\vec{k}\right) = f - f_0 = -\cos\theta_g \frac{\partial f_0}{\partial T} \frac{dT}{dx} M_A, \quad [3]$$

where $M_A = (1 - P_B)t_{BA} + P_B(1 - P_C)(t_{BA} + t_{CB}) + P_B P_C(1 - P_D)(t_{BA} + t_{CB} + t_{DC}) + \ldots$, $t_{BA}$ is the distance between point $A$ and the first reflection point on the boundary (point $B$), $t_{\Psi\Omega}$ is the distance between boundary reflection points $\Psi$ and $\Omega$, which can be point $B$, $C$, $D, \ldots$, and the subscript $g$ denotes the group velocity. In this calculation, phonons are traced along the direction of their group velocity to determine boundary reflection points, as shown in Fig. 5. In Eq. 3, $P_\Psi$ is a specularity parameter that represents the probability that phonons incident on the boundary point $\Psi$ undergo mirror reflection. This treatment satisfies the zero net heat flux condition across the interface (*SI Materials and Methods*).

Based on Eq. 3, the basal-plane thermal conductivity of supported MLG in the boundary scattering regime is calculated through:

$$\kappa_{BS} = \frac{1}{A_c} \sum_p \sum_{\vec{k}} |v_g| \ k_B \ x^2 \frac{e^x}{(e^x - 1)^2} \frac{\Delta k^3}{8\pi^3} (\cos\theta_g)^2 \int_{A_c} M \, dA_c, \quad [4]$$

where $v_g$ is the group velocity and $A_c$ is the cross-section of the MLG. Based on a numerical summation over the discretized Brillouin zone, this calculation has been carried out for a 34-layer-thick, 5.3-$\mu$m-wide, and 35.8-$\mu$m-long MLG sample with two diffuse side edges. As shown in Fig. 2, the calculation result can match the measurement result in the low temperature limit when the specularity is set to be either the same value of 0.36 for
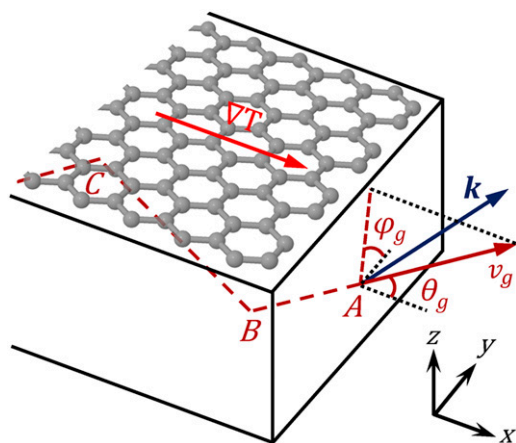
**Fig. 5.** Schematic used to derive the phonon-boundary scattering model in a MLG ribbon where the group velocity and wave vector are not collinear because of the highly anisotropic structure. In this schematic, $\theta$ and $\varphi$ are the polar angle with x-axis and the corresponding azimuthal angle in the $yz$-plane, respectively. The subscript $g$ is used to denote the group velocity.

the top and bottom surfaces of the MLG or 1 for a specular top surface and 0 for a diffuse bottom surface. The higher calculated thermal conductivity values than the measurement results at higher temperatures can be attributed to the ignorance of other scattering mechanisms in the calculation. Because the supported MLG samples underwent thorough cleaning process compared with suspended graphene and hexagonal Boron nitride (h-BN) samples reported in refs. 12 and 23 (*SI Materials and Methods*), the top surface is expected to be relatively clean and characterized with a higher specularity parameter than the bottom MLG–SiO$_2$ interface. Hence, the two sets of parameters presented here give the two limiting cases. The specularity parameter in the range between 0 and 0.36 found for the MLG–SiO$_2$ interface is in agreement with the high transmission coefficient shown in Fig. 4 at low temperatures and the expectation that the transmitted phonons contribute to the diffuse component.

Partially diffuse interface-phonon scattering can also explain the shift of the peak thermal conductivity to a lower temperature for a thicker MLG supported on SiO$_2$. The very high peak thermal conductivity value in graphite consists of a dominant contribution of low-frequency acoustic phonons (3), which possess considerably longer umklapp scattering mean free path than intermediate and high-frequency phonons. Even in the frequency-independent boundary scattering treatment presented above, the low-frequency phonons with a longer umklapp mean free path are subjected to a larger relative reduction in the mean free path than higher frequency phonons. Moreover, it has been suggested that the interface phonon transmission coefficient increases with decreasing phonon frequency (43). This frequency dependence is also revealed by the increased $\tau_{MLG \to SiO_2}$ value with decreasing temperature that we have calculated based on the $G_c$ values reported for encased FLG (41). Hence, interface transmission considerably reduces the thermal conductivity contribution from low-frequency phonons in supported MLG. Consequently, the relative contribution from intermediate and high-frequency phonons is higher in thinner supported MLG. Because of the increased population of intermediate and high-frequency phonons with increasing temperature, their thermal conductivity contribution in thin MLG increases with increasing temperature until a temperature where the umklapp scattering becomes as important as interface scattering for these phonons. Corresponding to the peak thermal conductivity, this temperature increases with decreasing MLG

thickness because of decreased mean free path for phonon scattering at the top and bottom interfaces.

The measurement and analysis show that partially diffuse interface scattering results in considerable suppression of the basal-plane thermal conductivity of MLG supported on amorphous oxide. Because of the long intrinsic mean free path of phonons, the suppression can be observed in supported MLG as thick as 34 atomic layers, and is more pronounced in thinner supported MLG. In comparison with MLG, a relative short intrinsic phonon mean free path in h-BN can also explain a recent measurement (23), which shows that the room-temperature basal-plane thermal conductivity of few-layer h-BN coated with polymer residue approaches the corresponding bulk value when the layer thickness is increased to be just 11 layers. In addition, based on the observed shift of the peak thermal conductivity to a higher temperature in thinner supported MLG, the interface scattering results in a large reduction of the mean free path of low-frequency acoustic phonons in supported MLG. Such reduction cannot be simply attributed to interface roughness scattering, which is known to be more effective in scattering higher frequency, shorter wavelength phonons (42). Instead, the reduction is largely influenced by interface phonon transmission, which is found to be nonnegligible based on the measured thermal interface conductance values and is known to increase with decreasing phonon frequency (43). Such interface scattering bears a resemblance to that revealed by past studies in phonon transport in thin film superlattices (44), where the phonon distribution in one layer is influenced by that of the adjacent layer when the interface is partially diffuse. Compared with thin film superlattices, the distinction lies in the highly anisotropic phonon structure in MLG, which gives rise to currently unknown mode coupling mechanisms across the interface. The interface coupling may be influenced by interface roughness. This knowledge gap calls for further studies of phonon transport at the interface of highly anisotropic materials, where new Snell's law awaits to be discovered. Advances along this direction may allow for a rational choice of the support materials to increase the basal-plane thermal conductivity of supported graphene.

## Materials and Methods

Although the device fabrication and measurement method are based on those reported in ref. 11 for thermal measurements of supported SLG samples, several notable changes have been made in the device design and measurement procedure for the 34-layer MLG sample (G34) to further reduce the relative error caused by contact thermal resistance, which is expected to increase with the MLG layer thickness. For increasing the area for heat transfer across the two ends of the MLG ribbon, each end of the 34-layer-thick MLG ribbon extends by 20 μm into the region between the straight RT line and the adjacent U-shape RT line, and is clamped between a top Cr/Au metal layer and the underlying SiO$_2$ beam. For increasing the thermal resistance of each straight RT line relative to its contact thermal resistance to the MLG, the metal line length and width of the straight RT lines are increased and decreased, respectively, compared to those of the U-shape RT lines. We used three-dimensional (3D) finite element models of the measurement devices to investigate the accuracy of the measurement method due to systematic errors caused by neglecting thermal contact resistances and thermal resistance of the substrate, and the assumption of uniform temperature across the thickness of the supporting SiO$_2$ beam. With the use of the largest thermal interface resistance value reported for different MLG and SLG samples (20) as well as the lowest reported cross-plane thermal conductivity and the highest reported in-plane thermal conductivity of graphite at different temperatures (2), the largest relative uncertainty is found in sample G27 at 100 K, where the basal-plane thermal conductivity is underestimated by no more than 9%. Moreover, the symmetry of the fabricated device is verified by two measurements each with a different U-shape RT line as the heater line (*SI Materials and Methods*). In addition, we have used a steady-state comparative method to measure the thermal conductivity of the NG source from which the MLG samples were exfoliated. The measurement setup consisted of a graphite bar of

$8 \times 1.6 \times 0.28$ mm$^3$ dimension bonded to a reference copper bar of $9.3 \times 1.8 \times 0.6$ mm$^3$ dimension. A thin film resistor attached to one end of the copper bar was used to generate temperature gradients in the copper bar and graphite bar, which were measured using two constantan-copper differential thermocouples of 0.003-inch diameter. The thermal conductivity of the graphite bar is obtained from the ratio of the thermovoltage differences, dimensions of the bars, and literature thermal conductivity of copper.

1. Slack GA (1962) Anisotropic thermal conductivity of pyrolytic graphite. *Phys Rev* 127(3):694–701.
2. Touloukian YS, Powell RW, Ho CY, Klemens PG eds (1970) *Thermophysical Properties of Matter* (IFI/Plenum, New York), Vol 2.
3. Klemens PG, Pedraza DF (1994) Thermal conductivity of graphite in the basal-plane. *Carbon* 32(4):735–741.
4. Baughman RH, Zakhidov AA, de Heer WA (2002) Carbon nanotubes—The route toward applications. *Science* 297(5582):787–792.
5. Geim AK (2009) Graphene: Status and prospects. *Science* 324(5934):1530–1534.
6. Tien CL, Majumdar A, Gerner FM (1998) *Microscale Energy Transport* (Taylor & Francis, Washington, DC).
7. Kim P, Shi L, Majumdar A, McEuen PL (2001) Thermal transport measurements of individual multiwalled nanotubes. *Phys Rev Lett* 87(21):215502.
8. Ghosh S, et al. (2010) Dimensional crossover of thermal transport in few-layer graphene. *Nat Mater* 9(7):555–558.
9. Marconnet AM, Panzer MA, Goodson KE (2013) Thermal conduction phenomena in carbon nanotubes and related nanostructured materials. *Rev Mod Phys* 85(3): 1295–1326.
10. Balandin AA (2011) Thermal properties of graphene and nanostructured carbon materials. *Nat Mater* 10(8):569–581.
11. Seol JH, et al. (2010) Two-dimensional phonon transport in supported graphene. *Science* 328(5975):213–216.
12. Pettes MT, Jo IS, Yao Z, Shi L (2011) Influence of polymeric residue on the thermal conductivity of suspended bilayer graphene. *Nano Lett* 11(3):1195–1200.
13. Lindsay L, Broido DA, Mingo N (2010) Flexural phonons and thermal transport in graphene. *Phys Rev B* 82(11):115427.
14. Jang WY, Chen Z, Bao WZ, Lau CN, Dames C (2010) Thickness-dependent thermal conductivity of encased graphene and ultrathin graphite. *Nano Lett* 10(10): 3909–3913.
15. Lindsay L, Broido DA, Mingo N (2011) Flexural phonons and thermal transport in multilayer graphene and graphite. *Phys Rev B* 83(23):235428.
16. Klemens PG (2001) Theory of thermal conduction in thin ceramic films. *Int J Thermophys* 22(1):265–275.
17. Ong ZY, Pop E (2011) Effect of substrate modes on thermal transport in supported graphene. *Phys Rev B* 84(7):075471.
18. Qiu B, Ruan XL (2012) Reduction of spectral phonon relaxation times from suspended to supported graphene. *Appl Phys Lett* 100(19):193101.
19. Chen J, Zhang G, Li BW (2013) Substrate coupling suppresses size dependence of thermal conductivity in supported graphene. *Nanoscale* 5(2):532–536.
20. Sadeghi MM, Pettes MT, Shi L (2012) Thermal transport in graphene. *Solid State Commun* 152(15):1321–1330.
21. Ong ZY, Pop E, Shiomi J (2011) Reduction of phonon lifetimes and thermal conductivity of a carbon nanotube on amorphous silica. *Phys Rev B* 84(16):165418.
22. Ferrari AC (2007) Raman spectroscopy of graphene and graphite: Disorder, electron-phonon coupling, doping and nonadiabatic effects. *Solid State Commun* 143(1-2): 47–57.
23. Jo I, et al. (2013) Thermal conductivity and phonon transport in suspended few-layer hexagonal boron nitride. *Nano Lett* 13(2):550–554.
24. Koenig SP, Boddeti NG, Dunn ML, Bunch JS (2011) Ultrastrong adhesion of graphene membranes. *Nat Nanotechnol* 6(9):543–546.
25. Aizawa T, et al. (1990) Phonon-dispersion in monolayer graphite formed on Ni(111) and Ni(001). *Surf Sci* 237(1-3):194–202.
26. Shikin AM, Farias D, Adamchuk VK, Rieder KH (1999) Surface phonon dispersion of a graphite monolayer adsorbed on Ni(111) and its modification caused by intercalation of Yb, La and Cu layers. *Surf Sci* 424(1):155–167.
27. Wu MC, Xu Q, Goodman DW (1994) Investigations of graphitic overlayers formed from methane decomposition on Ru(0001) and Ru(1120) catalysts with scanning-tunneling-microscopy and high-resolution electron-energy-loss spectroscopy. *J Phys Chem* 98(19):5104–5110.
28. Farias D, et al. (2000) Modification of the surface phonon dispersion of a graphite monolayer adsorbed on Ni(111) caused by intercalation of Yb, Cu and Ag. *Surf Sci* 454(1):437–441.
29. Aizawa T, et al. (1992) Phonon-dispersion of monolayer graphite on Pt(111) and NbC surfaces—Bond softening and interface structures. *Surf Sci* 260(1-3):311–318.
30. Yoon T, et al. (2012) Direct measurement of adhesion energy of monolayer graphene as-grown on copper and its application to renewable transfer process. *Nano Lett* 12(3):1448–1452.
31. Cullen WG, et al. (2010) High-fidelity conformation of graphene to SiO$_2$ topographic features. *Phys Rev Lett* 105(21):215504.
32. Lui CH, Liu L, Mak KF, Flynn GW, Heinz TF (2009) Ultraflat graphene. *Nature* 462(7271):339–341.
33. Meyer JC, et al. (2007) The structure of suspended graphene sheets. *Nature* 446(7131): 60–63.
34. Locatelli A, et al. (2010) Corrugation in exfoliated graphene: An electron microscopy and diffraction study. *ACS Nano* 4(8):4879–4889.
35. Giannozzi P, et al. (2009) QUANTUM ESPRESSO: A modular and open-source software project for quantum simulations of materials. *J Phys Condens Matter* 21(39):395502.
36. Shen M, Schelling PK, Keblinski P (2013) Heat transfer mechanism across few-layer graphene by molecular dynamics. *Phys Rev B* 88(4):045444.
37. Klemens PG (2000) Theory of the a-plane thermal conductivity of graphite. *Journal of Wide Bandgap Materials* 7(4):332–339.
38. Chen G (2005) *Nanoscale Energy Transport and Conversion: A Parallel Treatment of Electrons, Molecules, Phonons, and Photons* (Oxford Univ Press, Oxford).
39. Prasher R (2008) Thermal boundary resistance and thermal conductivity of multi-walled carbon nanotubes. *Phys Rev B* 77(7):075424.
40. Mak KF, Lui CH, Heinz TF (2010) Measurement of the thermal conductance of the graphene/SiO$_2$ interface. *Appl Phys Lett* 97(22):221904.
41. Chen Z, Jang W, Bao W, Lau CN, Dames C (2009) Thermal contact resistance between graphene and silicon dioxide. *Appl Phys Lett* 95(16):161910.
42. Ziman JM (1960) *Electrons and Phonons: The Theory of Transport Phenomena in Solids* (Clarendon, Oxford).
43. Prasher R (2009) Acoustic mismatch model for thermal contact resistance of van der Waals contacts. *Appl Phys Lett* 94(4):041905.
44. Chen G (1997) Size and interface effects on thermal conductivity of superlattices and periodic thin-film structures. *J Heat Trans-T Asme* 119(2):220–229.